MEASURING COLLECTED GAS WITH MICROWAVE AND ACOUSTIC RESONANCES

K A Gillis[1], J W Schmidt[1], J B Mehl[2], and M R Moldover[1]

[1] Sensor Science Division, National Institute of Standards and Technology, Gaithersburg, MD, 20899-8360 USA
[2] 36 Zunuqua Trail, PO Box 307 Orcas, WA 98280-0307, USA

E-mail: keith.gillis@nist.gov

Abstract

With calibrations of large flow meters in mind, we established the feasibility of determining the mass M of argon gas contained within a 0.3 m^3 commercially manufactured pressure vessel ("tank") with a relative standard uncertainty of $u_r(M) = 0.0016$ at 0.6 MPa by combining the measured argon pressure and the measured microwave and acoustic resonance frequencies within the pressure vessel with an accurate equation of state for argon.[1] This combination of measurements replaced the difficult problem of accurately measuring the average temperature of a large volume of gas with the easier problem of accurately measuring the average speed-of-sound in the gas. We heated the tank's top until it was 13 K warmer than its bottom. Remarkably, the temperature gradient changed the deduced mass by only (0.004 ± 0.026) %. We conclude that resonance frequencies can be used to "weigh" the compressed gas in much larger tanks, which might be made from ferromagnetic steel and possibly at high pressures in un-thermostatted environments. Details of this work have appeared in two previous publications. In the first, we used microwaves to determine the tank's internal volume V_{micro} with $u_r(V_{micro}) = 0.0006$ as well as the tank's thermal expansion (Moldover M R *et al*. 2015 *Meas. Sci. Tech*. **26** 015304). In the second publication, we showed that the microwave results accurately predicted the wavenumbers k_{calc} of the four lowest-frequency acoustic modes of the gas. (Gillis K A *et al.*, 2015 *Metrologia* **52** 337-352) We used these modes to determine the mass of the argon in the tank. The largest component of $u_r(M)$ resulted from the poorly understood interaction between the acoustic oscillations of the gas and the mechanical vibrations the tank's walls.

1. Introduction

In this exploratory work, we demonstrate how measurements of microwave and acoustic resonance frequencies and the pressure can be used to determine the mass of argon in a 0.3 m^3-volume of a commercially manufactured, un-thermostatted pressure vessel ("tank") made of ferromagnetic steel. (See Fig. 1.) In a previous publication [1], we reported a model for the shape and the volume [$V_{tank,micro} = 295.69 \times (1 \pm 0.0006)$ L] of the tank that we deduced from our measurements of the micro-

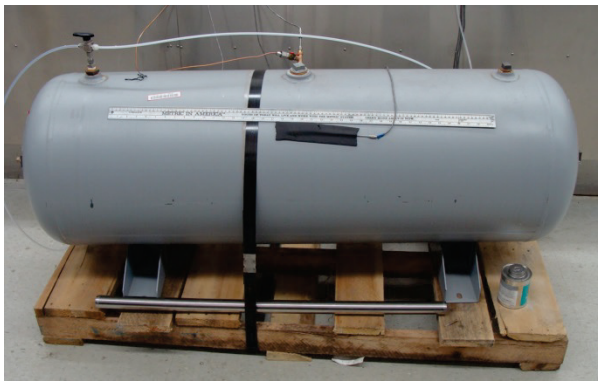

Figure 1. Photograph of the 1.6 m long pressure vessel configured for gas expansion measurements.

[1] All stated uncertainties are standard uncertainties corresponding to a 68 % confidence level.

wave resonance frequencies in the tank. In a second publication [2], we measured the acoustic resonance frequencies and the pressure and combined these measurements with our model of the shape of the tank to determine the average speed of sound u in the argon.[2] Then, we numerically inverted the full equation of state of argon given in [3], to determine the average mass density of the argon $\langle \rho(p,u^2) \rangle$. Finally, we determined the mass of the argon M from the product $M = \langle \rho(p,u^2) \rangle V_{\text{tank}}$ with a relative uncertainty $u_r(M) = 0.0016$.

The flow of information from the measurements and calculations to the mass is illustrated in Fig. 2. The relative uncertainty was estimated from the standard deviation of 4 values of M obtained with 4 low-frequency acoustic modes at a pressure near 0.6 MPa. The largest contributor to $u_r(M)$ was the poorly understood interaction between the acoustic modes of the gas and the frequency-dependent compliance of the tank's walls.

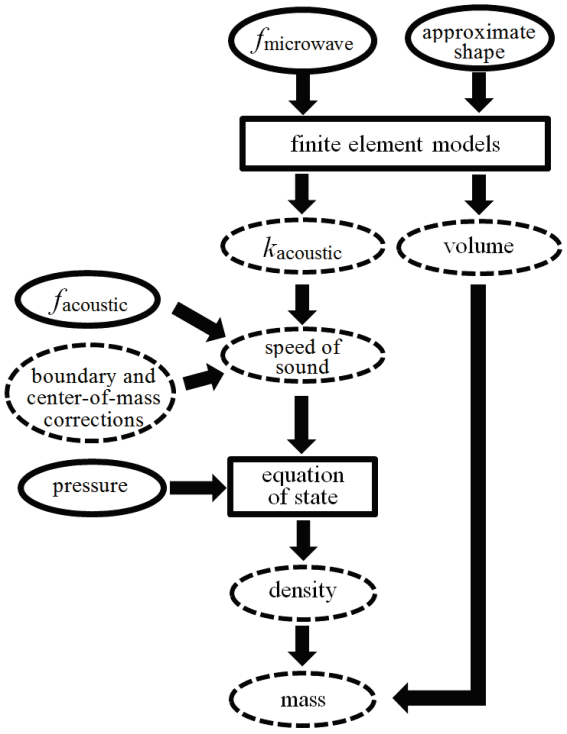

Figure 2. Outline of mass determination. Solid ovals indicate measured quantities; dashed ovals indicate computed quantities such as k_{acoustic} which are the wavenumbers of the resonant modes of the gas in the tank.

To gain insight into this technique to determine M, it is convenient to combine the virial expansion for the equation of state $p(\rho,T)$ with the pressure expansion of the speed of sound $u^2(p,T)$ to obtain the relation

$$M = \frac{\gamma_0 p V_{\text{tank}}}{u^2}\left[1 + (\beta_a - B)\frac{p}{RT} + \ldots\right] \quad , \tag{1}$$

where p is the pressure, $\gamma_0 \equiv C_p/C_V$ is the zero-pressure heat-capacity ratio, and β_a and B are the acoustic and the density virial coefficients, respectively. [4] Because the temperature appears only in the correction terms in Eq (1), we have replaced the difficult problem of accurately measuring the average temperature of a large volume of gas with the easier problem of accurately measuring the average speed-of-sound in the gas. In practice, we did not use truncated expansions for the equation of state and the speed of sound, as suggested by Eq (1). Instead, we used the full numerical equation of state from [3].

The acoustic wavenumbers of a resonant cavity are insensitive to linear temperature gradients (in the first order of perturbation theory); therefore, resonance determinations of the speed of sound are only weakly dependent on temperature gradients in the gas. [Remarkably, heating the tank's top until it was 13 K warmer than the tank's bottom increased the acoustic frequencies of the lowest three non-degenerate modes by $\Delta f_{\text{meas}}/f_{\text{meas}} = (0.2 \pm 1.3)\times 10^{-4}$. See column "meas" in table 2.] The acoustic and microwave techniques that we used are scalable to very large volumes; therefore, we anticipate resonance techniques

[2] In this paper we use u for speed of sound, c for the speed of light in vacuum, and u_r for relative uncertainty.

will be used to weigh compressed gas in much larger tanks, at higher pressures, and in un-thermostatted environments. Such a large tank could be used as a gas source and/or a gas collector during the calibration of large gas-flow meters. We expect that these techniques will also be used to solve other problems in large-scale gas metrology.

In the remaining numbered sections of this paper we provide an overview of the following subjects: (2) description of the tank, (3) using microwaves to determine the tank's volume and shape, (4) isothermal acoustic measurements of resonance frequencies, (5) determining the mass of the gas in the tank, including effects of temperature gradients, and (6), the prospects for scaling up the present ideas to make a useful flow standard. Details may be found in Refs. [1] and [2].

We conclude this Introduction by emphasizing that our goal was to explore the phenomena that will be encountered if and when a large tank is incorporated into a flow standard; therefore, we did not make extensive efforts to characterize the tank in Fig. 1 as accurately as possible.

2. The Tank

Here, we describe the tank using information provided by the manufacturer, and we mention the gas-expansion measurements that were used in [1] to confirm the microwave measurements of the volume (see Section 3).

2.1. Construction of the tank

The tank was commercially manufactured for use as an air receiver with a maximum operating pressure of 1.38 MPa (Silvan Industries[3], Inc., Marinette, WI, USA, Part Number A10031). The manufacturer stated that it was designed and built to comply with ASME Code, Section VIII, Div. 1, 20th Edition. The tank was manufactured from the ferromagnetic, hot-rolled carbon steel alloy SA414-G. As shown in figure 1, the tank was a horizontal, approximately circular cylinder with hemispheroidal "end caps" (called "heads") welded to each end of the cylinder. The manufacturer's drawings indicate that the cylindrical section has a length of 1.3 m, a diameter of 0.51 m, and a wall thickness of 3.9 mm. The cylindrical section had been manufactured from a plate, and it had a weld bead along its entire length on both its outside and inside surfaces. The end caps were "2:1 semielliptical heads." Their shapes were approximately oblate hemispheroids (that is, half of an ellipse of revolution) with a 0.12 m semi-minor axis and a 3.2 mm wall thickness. The end caps had a joggle (a short cylindrical extension that fit inside the cylindrical section) to facilitate welding. We estimated that the joggles plus the weld beads inside the tank occupied approximately 130 cm^3 $\approx$ 0.00043 V_{tank} in the tank interior. We did not modify the tank for this research.

The tank's walls were penetrated by 7 ports. At each port, the manufacturer had welded a threaded fitting to the outside of the tank. We inserted the acoustic transducers into the two ports near either end of the top surface of the tank. As described in [1], microwave antennas were installed in two other ports and a thermometer was installed in a fifth port. We capped the remaining two ports, located on the axis of each end cap, with threaded brass plugs that were sealed with polytetrafluoroethylene (PTFE) tape. One port

[3] In order to describe materials and procedures adequately, it is occasionally necessary to identify commercial products by manufacturers' name or label. In no instance does such identification imply endorsement by the National Institute of Standards and Technology, nor does it imply that the particular product or equipment is necessarily the best available for the purpose.

was unused, and the other was connected to the argon source. They were the largest ports and, when capped, each had an internal volume of approximately 30 cm^3. The internal volumes of the 5 smaller ports totaled 29 cm^3.

2.2. Measuring the volume by gas expansion

As a reference, we determined the volume of the tank V_{tank} at ambient temperature using a gas-expansion technique that requires a well-thermostatted, accurately known standard volume V_{std}. Details of this technique are given in [1]. Initially, the tank was filled with pure nitrogen at the measured pressure $p_{tank,i}$ and at the temperature $T_{tank,i}$ while the standard volume was evacuated to the low measured pressure $p_{std,i}$ at the temperature $T_{std,i}$. Then, a valve in a tube connecting the standard volume to the tank was opened and both volumes were allowed to equilibrate. Finally, the pressure p_f and temperatures $T_{std,f}$ and $T_{tank,f}$ were measured. Conservation of the nitrogen's mass leads to the approximate relationship between V_{tank} and V_{std}

$$M_{N2} \approx \rho_{std,i} V_{std,i} + \rho_{tank,i} V_{tank,i} \approx \rho_{std,f} V_{std,f} + \rho_{tank,f} V_{tank,f} \quad , \tag{2}$$

where the four densities were calculated from the corresponding temperature and pressure measurements using the virial equation of state for nitrogen. [5]

For V_{std}, we used the collection volume of NIST's flow standard. Wright *et al*. used gravimetric methods to determine V_{std} = (677.936 ± 0.028) L when the temperature was 296.655 K. [6] During the present measurements, the water bath that thermostats V_{std} was always within ±0.004 K of 296.655 K.

The dominant contributor to the uncertainty of the gas-expansion method (up to 82 %) is the resolution of the pressure sensor on V_{tank}. The uncertainty of V_{tank} includes additional contributions from the pressure uncertainty in V_{std} and the uncertainty of the temperature change in the test tank from 4 thermistors.

Table 1. Measurements of the tank's internal volume at ambient temperature and ambient internal and external pressure. These results are plotted in Fig. 1.

Row	Method	Volume / liter
	Gas expansion	
1	100 kPa to 30 kPa	295.801±0.052
2	100 kPa to 30 kPa	295.788±0.052
3	30 kPa to 10 kPa	295.794±0.157
4	30 kPa to 10 kPa	295.699±0.157
	Microwaves	
5	3 Models; 3 param	295.69±0.18

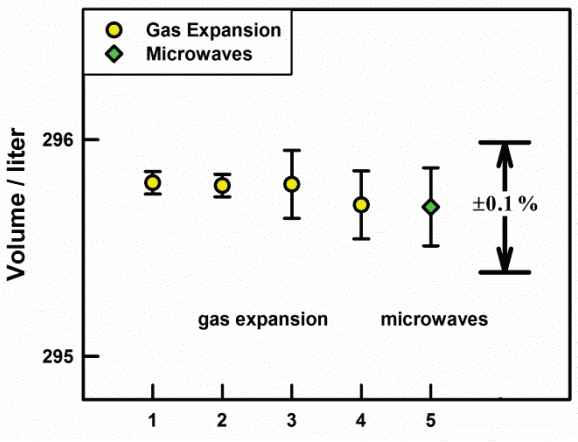

Figure 3. Results of volume measurements. The numbers on the horizontal axis correspond to the rows in Table 1. Data from Sect. 2 ○, gas-expansion; Sect. 3 ◆, microwaves.

The volume of the tank measured with the gas-expansion method was computed as the weighted average from 4 expansions, listed in rows 1 to 4 in Table 1 and plotted in Fig. 3, with the result

$$V_{\text{tank,gas}} = (295.790 \pm 0.052)\ \text{L} \quad . \tag{3}$$

In Eq. (3), we added the subscript "gas" to emphasize that the gas-expansion measurement determined the total volume of the tank that was accessible to the nitrogen gas. Therefore, $V_{\text{tank,gas}}$ includes small volumes that were not included in the models used to interpret the microwave and acoustic measurements.

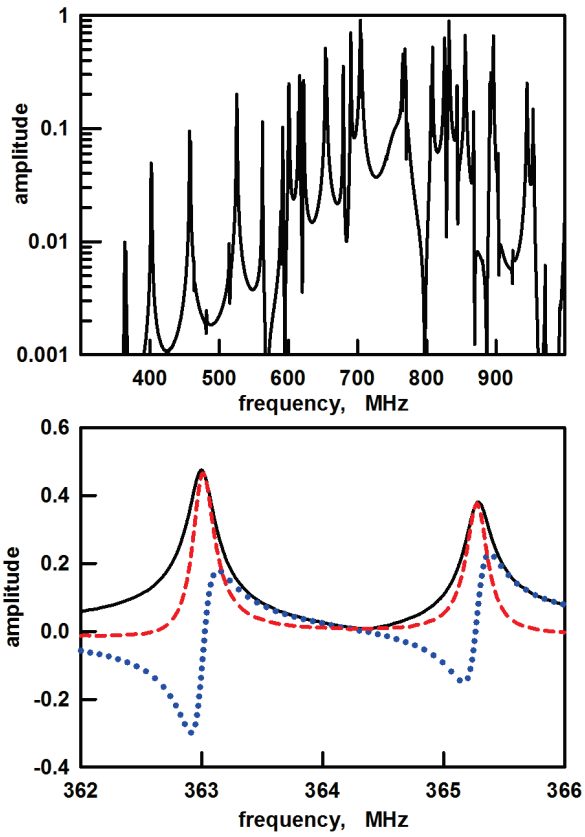

Figure 4. Microwave measurements. Top: Microwave amplitude on log scale from 350 MHz to 1000 MHz. The peaks are reproducible resonances, not noise. Bottom: Expanded spectrum of the TE111 doublet near 364 MHz measured with a vector analyzer. The red dashed line indicates the in-phase signal, the blue dotted line indicates the quadrature signal, and the black solid line indicates the computed amplitude.

3. Microwave Measurements and Analysis

3.1. Microwave frequency spectrum

Figure 4 displays the spectrum of the microwave resonances measured in the tank shown in Fig. 1. This spectrum was measured while the tank was filled with dry nitrogen at approximately 99 kPa and 22 °C. Under these conditions, the square of the refractive index of the nitrogen was $n_g^2 = 1.00053$.

The lower-frequency resonances in the top panel of Fig. 4 can be identified with the resonance modes of an ideal cylindrical cavity with flat ends. Following conventional derivations in the literature, for example [7, 8, or 9], we divide the resonance modes into two categories: transverse magnetic (TM) and transverse electric (TE), according to which field (magnetic or electric, respectively) has its axial component identically equal to zero. We impose boundary conditions on the microwave fields assuming the walls of the tank are perfectly conducting. For the TM*mnl* modes in an ideal cylindrical cavity, the resonance frequencies are:

$$\left(2\pi f_{\text{mnl}}^{\text{TM}}\right)^2 = \frac{c^2}{n_g^2}\left(\frac{l^2\pi^2}{L^2} + \frac{\alpha_{\text{mn}}^2}{a^2}\right) . \tag{4}$$

In Eq. (4), c is the speed of light in vacuum; n_g is the refractive index of the gas in the cavity; $l \geq 0$ is an integer; α_{mn} is the nth root of $J_m(z) = 0$; and J_m is the Bessel function of the 1st kind of order m. The resonance frequencies for the TE*mnl* modes of an ideal cylindrical cavity are given by an expression similar to Eq. (4), except the integer $l \geq 1$ and α_{mn} is replaced by β_{mn}, the nth root of $dJ_m(z)/dz = 0$.

Because the walls of our tank have a finite electrical conductivity σ_s and a relative magnetic permeability μ_s, the microwave fields within the walls decay exponentially with the decay length ("skin depth")

$$\delta_s = 1/\sqrt{\pi\mu_0\mu_s\sigma_s f} \quad . \tag{5}$$

Equation (5) predicts $\delta_s = 1.5\times10^{-6}$ m when $f = 400$ MHz, $\sigma_s = 4\times10^{6}$ S/m, and $\mu_s = 64$ using the electrical conductivity for the ferromagnetic alloy SA414-G and the relative permeability deduced from our microwave measurements. The vacuum permeability $\mu_0 = 4\pi\times10^{-7}$ N A^{-2} is a fundamental constant. The microwave fields within the skin depth reduce the resonance frequencies and increase the resonance half-widths by equal amounts g that are calculable from theory. Expressions for g for TM and TE modes are given by Eqs. (7) and (9) in [1].

Because the microwave fields extend into the tank's walls a distance on the order of δ_s, the microwave frequencies will overestimate the tank's volume by a fraction of order $\delta_s A_{tank}/V_{tank} \approx 1.3\times10^{-5}$, where A_{tank} is the internal surface area of the tank. We account for this overestimate by determining the dimensions of the tank from the sum ($f_{meas} + g_{meas}$) instead of from f_{meas} alone. We estimate the uncertainty in the volume due to the skin depth $u_r(\delta_s)$ $\delta_s A_{tank}/V_{tank} \approx 6\times10^{-6}$, which appears in Table 3.

3.2. Non-circular cross-section

In figure 1, the tank looks as if it had a horizontal axis of rotational symmetry. In microwave cavities that have an axis of rotational symmetry, the TE and TM modes with $m > 0$ can each have two independent orientations (about the cylinder axis) with exactly the same frequency; we say they are degenerate with multiplicity 2 or "doublets". Certain imperfections of the rotational symmetry will cause the frequencies of a degenerate doublet to separate from each other. If the imperfection is small, resonance peaks may partially overlap; if the imperfection is larger, the peaks are well-separated (by more than their combined widths). As shown in the lower panel of Fig. 1 (See Section 5.3 of [1].), the doubly degenerate microwave modes of this tank were separated (split) into easily resolved components. The splitting of the TE11*l* doublets was consistent with an elliptical cross section with semi-major axis $a(1+e)$, semi-minor axis $a/(1+e)$, and $e \approx 0.0026$. However, the splittings of other doublets provided evidence that the cross section was more complicated than elliptical. Known complications include the ports on the top of the tank; another plausible complication arises if there is a cusp at the weld parallel to the tank's axis that sealed the rolled plate into a cylindrical shape. (See Fig. 5)

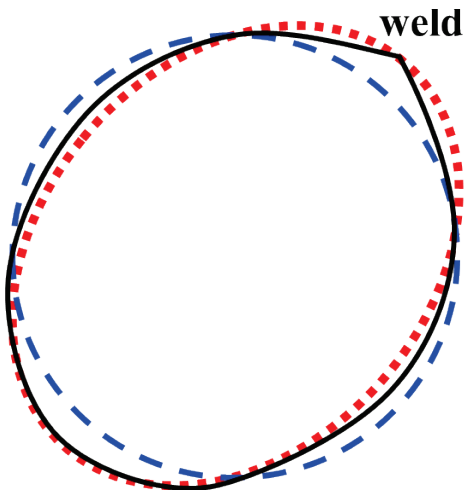

Figure 5. The dashed blue curve represents the circular cross-section of an ideal tank. The cross-section of a real tank might be elliptical (red dotted curve) and/or have a cusp at the weld (black curve).

Instead of searching for a model for the non-circular shape that was consistent with all the measured splittings, we averaged the measured doublet frequencies and then fitted them by models with circular cross sections. After averaging, any remaining effects of the non-circular shape will be of order

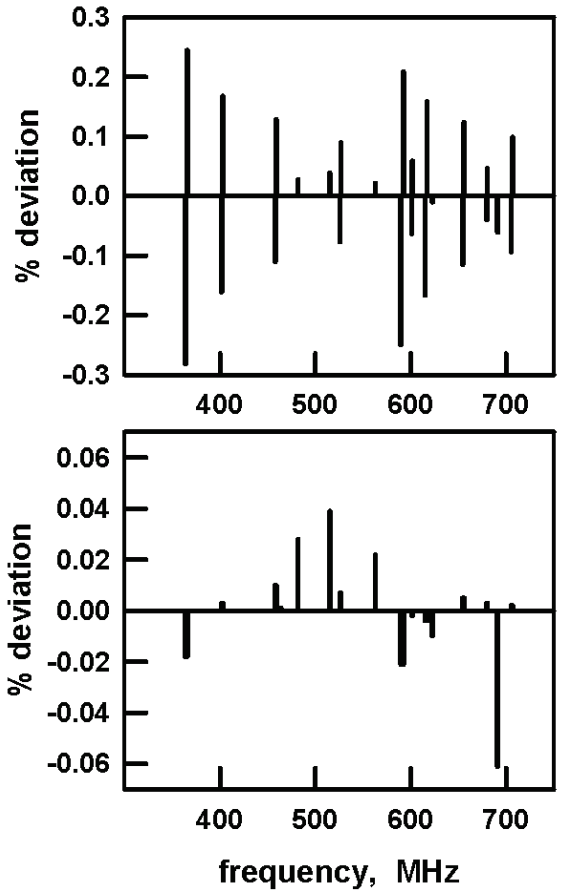

Figure 6. Top: deviation of 26 frequencies from the best fit of L, a, and b to the photo-based shape. For each doublet, the deviations have nearly equal positive and negative values. For 26 frequencies, the fractional standard deviation from the fit is $\sigma(\Delta f/f) = 0.0014$. Bottom: Same data as top, except that the frequencies of each doublet were averaged before fitting. The pre-averaging reduced $\sigma(\Delta f/f)$ from 0.0014 to 0.00019, a factor of 1/7.4.

e^2. In principle, these effects could be calculated using second-order shape perturbation theory [10]. Fortunately, for values of $e \sim 0.0026$, the second-order perturbations will be negligible compared with other errors. The benefit of averaging the frequencies of doublets before fitting with a model shape is demonstrated in Fig. 6, which shows a factor of 7 reduction in the fractional deviations of the measured frequencies from a best fit.

3.3. Determining the volume and shape

The lower panel of Fig. 4 displays an expanded view of the frequency-dependence of the in-phase and quadrature components of the microwave voltage detected near the TE111 using a microwave vector analyzer. The vector analyzer data were fitted by complex-valued resonance formula as described in [11]. The two-fold nearly-degenerate modes, (such as the TE111 mode shown in Fig. 4) were easily fitted with a vector sum of two resonance formulas. The fitted values of f_{res} and g_{res}/f_{res} had relative uncertainties $u_r(f) < 10^{-6}$ and $u_r(g/f) < 10^{-6}$. For the microwave determination of the volume V_{micro}, these uncertainties are insignificant compared with the uncertainty resulting from imperfect knowledge of the tank's shape.

We used the 16 lowest-frequency modes of the tank to determine V_{micro}. Of these modes, 10 were nearly degenerate doublets and 6 were non-degenerate singlets spanning the range 363 MHz to 706 MHz. At higher frequencies, it became increasingly difficult to identify the measured frequencies with particular calculated frequencies because the density of modes and their widths increase as the frequency increases, so the chance of the modes overlapping increases.

In [1] we correlated the measured spectrum of microwave resonances using three models for the shape of the tank. Our best estimate of the tank's volume from the microwave measurements was $V_{tank,micro} = 295.69 \times (1 \pm 0.0006)$ L.[4] As described here in Section 2 and in [1] in more detail, we also measured the internal volume of the tank using an accurate gas-expansion method and obtained the result $V_{tank,gas} = 295.790 \times (1 \pm 0.00017)$ L, where the uncertainty was dominated by imperfect pressure and temperature measurements. Thus, the microwave measurements and the more-accurate gas expansion measurements,

[4] Ref. [2] reports slightly incorrect values for $V_{tank,micro}$ and $V_{tank,gas}$. The correct values are reported here and in [1].

which shared neither theory nor instruments, yielded consistent results within combined uncertainties. The gas-expansion measurement of $V_{\text{tank,gas}}$ required careful measurements of temperature differences; in contrast, the temperature entered into the microwave measurement of $V_{\text{tank,micro}}$ only through the tank's thermal expansion: $(\partial V/\partial T)_p/V = (35.3 \pm 1.9)\times10^{-6}\ \text{K}^{-1}$. Therefore the microwave measurement of $V_{\text{tank,micro}}$ could tolerate a temperature uncertainty of 10 K without significantly increasing the uncertainty of $V_{\text{tank,micro}}$.

After averaging the doublets, the simplest shape that was consistent with the microwave frequencies was a tank with a cylindrical center section of length L and hemispheroidal end caps with a semi-minor axis b and two semi-major axes of length a, where a is also the radius of the central section. This model has three parameters (L,a,b) and the volume $V = \pi a^2(L + 4b/3)$. The best-fit values were L = 1.34154 m, a = 0.25021 m, b = 0.12129 m. We used this model shape as an input to commercial, finite-element (FE) software [12,13] to calculate the acoustic resonance frequencies of the tank.

3.4. Measuring the Thermal and Pressure Expansion of the Tank.

3.4.1. Thermal Expansion

We estimated the thermal expansion of the tank from the values of $(f_{\text{meas}} + g_{\text{meas}})$ for 11 microwave modes while the laboratory thermostat was set at two different temperatures: $T_1 \approx 19$ °C and $T_2 \approx 22$ °C. For the 11 modes, we computed the ratios

$$\Re = (f+g)_{T1} / (f+g)_{T2} \quad . \tag{6}$$

[For the doublets, the values of $(f_{\text{meas}} + g_{\text{meas}})$ were averaged before calculating $\Re$.] The average and standard deviation of $\Re = 1 + (34.44 \pm 0.19)\times10^{-6}$. Remarkably, the values of $\Re$ were the same for TE and TM modes and had no detectable frequency-dependence. These observations imply that the thermal expansion of the tank was isotropic, a result that is expected because the tank was made entirely from one alloy.

During the thermal expansion measurements, the tank was evacuated and the change in the tank's temperature was inferred from three thermometers that we calibrated. For computing the thermal expansion, we assumed that the temperature change was the average of the thermistor readings (2.93 ± 0.16) K, where the uncertainty was the range spanned by the three thermometers. With these assumptions and the observed isotropy, the linear coefficient of thermal expansion is $\alpha_T = (11.75 \pm 0.64)\times10^{-6}\ \text{K}^{-1}$ and the thermal expansion coefficient of the volume is

$$(\partial V / \partial T)_p / V = 3\alpha_T = (35.3 \pm 1.9)\times10^{-6}\ \text{K}^{-1}. \tag{7}$$

Our result for α_T agrees with the value $11.5\times10^{-6}\ \text{K}^{-1}$ reported for carbon steel SA414-G in [14].

3.4.2. Pressure expansion

We attempted to measure the pressure expansion of the tank; however, the results led to an unsolved puzzle. We measured $[f_N(p,T) + g_N(p,T)]$ for 15 microwave modes at 3 pressures when the tank was near 22 °C, after first averaging the frequencies of the doublets. Surprisingly, the average $\langle (df_N/dp)/f_N \rangle$ for the TM modes differed from the average for the TE modes, and furthermore, suggested that the expansion

was anisotropic. However, we were unable to interpret the results using the FE software to calculate the partial derivatives of $f_N(L,a,b)$ with respect to the lengths L, a, and b in our 3-parameter model for the tank.

Since we were unable to obtain a sensible measurement of the pressure expansion, we estimated an upper bound of $(1/V)(dV/dp) = 0.62\times10^{-6}$ kPa^{-1} for a long cylinder using a formula from [15]. This estimate predicts the fractional increase in tank's volume at its maximum working pressure (1.38 MPa) is $\Delta V/V = 0.00086$. Therefore, the volume that we determined while the tank was evacuated is a good approximation to the volume at any pressure up to the maximum working pressure. (The same volume change, $\Delta V/V = 0.00086$, would occur if the temperature of the tank were increased by 24 K.)

4. Acoustic Measurements and Analysis

As a first approximation, we calculated the acoustic spectrum using a right circular cylindrical cavity with radius a = 25 cm and length L = 150.34 cm; the length was chosen to make the volume of the cylinder equal to the volume of the tank. This cylindrical approximation provides: (1) a notation that identifies the lower-frequency acoustic modes, (2) estimates of the half-widths of the acoustic modes, (3) a model for calculating the dependence of the frequencies on temperature gradients, and (4) exact results that we used to test our implementation of the finite element (FE) software packages. We emphasize that the cylindrical cavity does not predict the acoustic wavenumbers with sufficient accuracy to determine the mass of the collected gas. In the next section 4.2, we explain how we accurately calculated the wavenumbers using finite element numerical methods.

4.1. Theoretical acoustic spectrum of a gas in a cylindrical shell

The unperturbed resonance frequencies $f^{(0)}_{\ell mn}$ of the acoustic modes of a gas in an ideal, perfectly cylindrical cavity surrounded by a rigid shell (the tank's walls) are given by

$$\left(\frac{2\pi f^{(0)}_{\ell mn}}{u}\right)^2 = K^2_{\ell mn} \equiv \left(\frac{\ell\pi}{L}\right)^2 + \left(\frac{\beta_{mn}}{a}\right)^2 \quad . \tag{8}$$

In Eq. (8) u is the speed of sound in the gas; $K_{\ell mn}$ is an acoustic eigenvalue (wavenumber); β_{mn} is the n^{th} root to $dJ_m(z)/dz = 0$ counting the first root with $n = 0$, and where $J_m(z)$ is the m^{th} order Bessel function; and ℓ, m, and n are non-negative integers. The triplet of indices (ℓmn) specifies the acoustic mode with longitudinal index ℓ, azimuthal index m, and radial index n.

Equation (8) neglects the non-zero thermal conductivity κ and the non-zero shear viscosity η of the gas. These transport properties lead to well-understood energy losses at the gas-shell boundary that generate a thermal contribution g_T and a viscous contribution g_v to the resonance half-widths $g_{\ell mn}$. They also reduce the resonance frequency f_{lmn} by $g_T + g_v$. The partial half-width g_T is proportional to the length $\delta_T \equiv [\kappa/(\rho C_p \pi f)]^{1/2}$, which is the thickness of the gas layer near the wall where heat conduction losses occur. (ρC_p is the gas's constant-pressure heat capacity per volume.) Similarly, the partial half-width g_v is proportional to $\delta_v \equiv [\eta/(\rho\pi f)]^{1/2}$, which is the thickness of the gas layer where viscous losses occur. (The

lengths δ_T and δ_v are analogous to the skin depth for microwaves.) Explicit mode-dependent expressions for g_T and g_v are given by Eqs. (4) and (5) in [2]. We used the calculated quantities g_T, g_v, and others described below to correct the measured resonance frequencies of the tank in order to improve the consistency among the modes and to improve the agreement with our FE calculations.

Equation (8) neglects also the interaction between the acoustic pressure oscillations and the shell. This interaction produces rigid-body motion and dynamic elastic deformations of the shell that perturb the resonance frequencies. The center-of-mass (CM) of a free-body shell oscillates out of phase with the gas for gas modes in which the gas's CM also moves. The CM motion of the shell increases the resonance frequency of the affected gas mode by an amount that is proportional to $M_{\text{gas}} / M_{\text{shell}}$. Equations (7) and (8) in [2] give analytic expressions for the frequency shifts $\Delta f_{\text{CM},1} \big/ f_{\ell 00}^{(0)}$ for longitudinal modes with odd-integer ℓ and $\Delta f_{\text{CM},2} \big/ f_{01n}^{(0)}$ for transverse modes (01n). The frequencies of the (ℓ00) modes where ℓ is an even integer and the frequencies of (0mn) modes with $m > 1$ are unchanged.

Our tank was loosely fastened to a wooden shipping pallet (figure 1); therefore, we expected that it would oscillate as a free body when driven by the acoustic oscillations of the gas within it. When the tank was at ambient temperature and filled with argon at 0.6 MPa, the ratio $M_{\text{gas}} / M_{\text{shell}}$ was 0.03710; under these conditions, the relative frequency increases predicted for the (1,0,0), (3,0,0), and (0,1,0) gas modes in a rigid cylindrical shell are 0.0150, 0.00167, and 0.0155, respectively. For comparison, we calculated $\Delta f_{\text{CM},1} \big/ f_{\ell 00}^{(0)}$ and $\Delta f_{\text{CM},2} \big/ f_{010}^{(0)}$ numerically with finite-element software (COMSOL 3D, FlexPDE) [12,13] using the ellipsoidal end-cap model for the tank's shape that we determined from microwave measurements [1]; the numerical calculations predict increases of 0.0151, 0.00172, and 0.0154 for the (1,0,0), (3,0,0), and (0,1,0) modes, respectively, which are remarkably close to the analytic predictions for a perfect cylinder.

We did not attempt to develop an analytic model for the dynamic deformations of a cylindrical shell in response to sound waves in the enclosed gas. Instead, we treated the elastic response of the shell as an empirical frequency perturbation Δf_{recoil} that was proportional to $(\rho u^2)_{\text{gas}}$ such that the coefficient of proportionality might have a complicated frequency dependence.

The effects CM,1 and CM,2 as well as Δf_{recoil} are proportional to the density of the gas; hence they are nearly proportional to the pressure. We combine the listed perturbations to obtain an expression for the measured frequencies $f_{\ell mn,\text{meas}}$

$$f_{\ell mn,\text{meas}} = f_{\ell mn}^{(0)} - g_T - g_v + \Delta f_{\text{recoil}} + \Delta f_{\text{CM},1} + \Delta f_{\text{CM},2} \quad . \tag{9}$$

We used $\Delta f_{\text{CM},1} \big/ f_{\ell 00}^{(0)}$ and $\Delta f_{\text{CM},2} \big/ f_{01n}^{(0)}$ for a cylindrical shell to estimate the effects CM,1 and CM,2 in our tank using the value $M_{\text{shell}} \approx 86$ kg, which was provided by the manufacturer and includes the 10 cm high "saddle legs" welded to the tank. A comparison of Figs. 9(a) and 9(b) below shows that $\Delta f_{\text{CM},1} \big/ f_{\ell 00}^{(0)}$ and $\Delta f_{\text{CM},2} \big/ f_{01n}^{(0)}$ account for nearly all the pressure-dependence of the frequencies of the (100), (300), and (010) modes.

Although useful for identifying the measured modes in our tank, Eq. (8) for a perfectly cylindrical cavity does not predict the acoustic wavenumbers with sufficient accuracy. As described in the next section, we calculated the wavenumbers numerically with finite element methods using the shape of tank that we deduced from the microwave measurements.

4.2. Finite-element calculations of the acoustic spectra of gas-filled model tanks.

We calculated the acoustic wavenumbers of gas modes in the tank's cavity using two different numerical methods. We also found nearly identical results for two differently shaped cavities. The differences between the results from these calculations are much smaller than other uncertainties.

We used the FlexPDE software [13] to calculate the acoustic wavenumbers of two model cavities that were used in [1] to analyze the microwave frequencies. Both model cavities had cylindrical center sections; one had spheroidal end caps and the second had axisymmetric end caps with shapes deduced from a photograph. (See table 2.) The wavenumbers calculated using the FlexPDE software for these 2D axisymmetric models differed by no more than 0.02 % for values of the wavenumber $k_{\ell mn} = 2\pi f_{\ell mn}/u$ spanning the range from 2 m^{-1} to 11 m^{-1}. (These values of k correspond to 100 Hz < $f_{\ell mn}$ < 600 Hz when the tank was filled with argon at 20 °C and 100 kPa.) We also used the COMSOL software [12] to calculate the wavenumbers for the photo-based profile using a full three-dimensional model formulation. For the nine lowest-frequency modes, the COMSOL 3D wavenumbers averaged 0.001 % higher than the 2D FlexPDE wavenumbers. This excellent agreement gave us confidence in the accuracy of the wavenumbers calculated using the FE software. (Both numerical methods assume that the walls of the tank are rigid and neither method includes the perturbations from the viscosity and thermal conductivity of the gas discussed in Section 4.1.)

Table 2. Calculated and measured wave numbers and calculated Qs of low-frequency gas modes. For the doublet modes, the wavenumbers have been averaged. The values of $Q_{\rm cyl}$ are calculated for 296 K. and 0.2 MPa.

mode	$k_{\rm ref}/{\rm m}^{-1}$	$10^4(k/k_{\rm ref}-1)$				$Q_{\rm cyl}$
	spheroidal	photo	cylinder	measured		0.2 MPa
				0 MPa	0.6 MPa	
1,0,0	2.08924	–2.7	–8.6	0.7	2.2	829
2,0,0	4.17465	–2.6	0.5	–3.8	–10.5	1172
3,0,0	6.25178	–2.5	17	–10.7	–13.2	1435
0,1,0	7.44209	–0.8	–104	2.6	–22.4	1726
1,1,0	7.83464	–1.8	–230	–1.5	74.2	1483
4,0,0	8.31446	–2.5	42			1657
2,1,0	8.67212	–2.0	–238	–17.0	–23.2	1485
3,1,0	9.88584	–1.6	–221			1512
5,0,0	10.3523	–3.0	82			1853
4,1,0	11.3578	–0.6	–197			1562
0,2,0	12.2865	–1.3	–57	9.6	57.2	1684

Table 2 summarizes many of the results of this section. For comparisons, the column $k_{\rm ref}$ lists the 11 smallest wavenumbers calculated for the cylindrical cavity with spheroidal end caps. The column "photo" compares $k_{\rm ref}$ with the wavenumbers for a cylindrical cavity with end cap shapes determined from a photograph. The column "cylinder" compares $k_{\rm ref}$ with the wavenumbers of a cylindrical cavity with the same volume. The measured values of k are discussed in Section 4.3. The column "$Q_{\rm cyl}$" lists the values of $Q = f_{\rm calc}/[2(g_v + g_T)]$ calculated using Eq. (8) and Eqs. (4) and (5) in [2] for an ideal cylinder at 0.2 MPa and 296 K. For the present measurements, a useful approximation is $Q_{\rm calc} = Q_{\rm cyl} \times (p/0.2\ {\rm MPa})^{1/2} \times (T/296\ {\rm K})^{-2/3}$.

4.3. Isothermal Measurements of Shell Resonances and Gas Resonances

In this section, we use wide-range isothermal scans of the acoustic spectra to identify the resonance modes of the empty tank (the "shell") and the resonance modes of the gas. The frequencies of the shell modes have a strong pressure-dependence; therefore, many will "cross" the frequencies of gas modes. For frequencies near mode crossings (known as "avoided crossings" in optical spectroscopy), the shell and the gas interact strongly. Because we lack an accurate theory for the complicated shell motion, modes that have such crossings cannot be used for gas metrology. After the overview, we discuss accurate measurements of the frequencies f_{meas} and half-widths g_{meas} of the acoustic (gas) modes at 0.2 MPa, 0.4 MPa, and 0.6 MPa. For many gas modes, the differences between f_{meas} and the FE-calculated frequencies f_{calc} tend to zero as the pressure tends to zero. For the three lowest-frequency gas modes, $|f_{meas}/f_{calc} - 1| < 1.4\times10^{-3}$ between 0 MPa and 0.6 MPa, provided that the center-of-mass frequency corrections (see Section 4.2) are made. Any one of these modes could determine the mass of the gas in the cavity with a relative uncertainty on the order of 2.8×10^{-3}. The remaining gas modes had large, un-modeled pressure-dependencies which limit their usefulness for gas metrology.

4.3.1. Overview

Figure 7 is a scan of the tank's acoustic spectrum measured under three different conditions: (1) evacuated with a mechanical pump, (2) filled with argon at 19 °C and 118 kPa, and, (3) filled with argon at 21 °C and 337 kPa. (To avoid overlapping curves, the amplitude of the vacuum spectrum was divided by 100 and the amplitude of the 337 kPa spectrum was multiplied by 100.)

As indicated in Fig. 7, all of the acoustic modes were detected near the frequencies predicted by the FE models, except for the (4,0,0) mode. The signal from the (4,0,0) mode was too small to detect because the transducers happened to be located near pressure nodes of that mode.

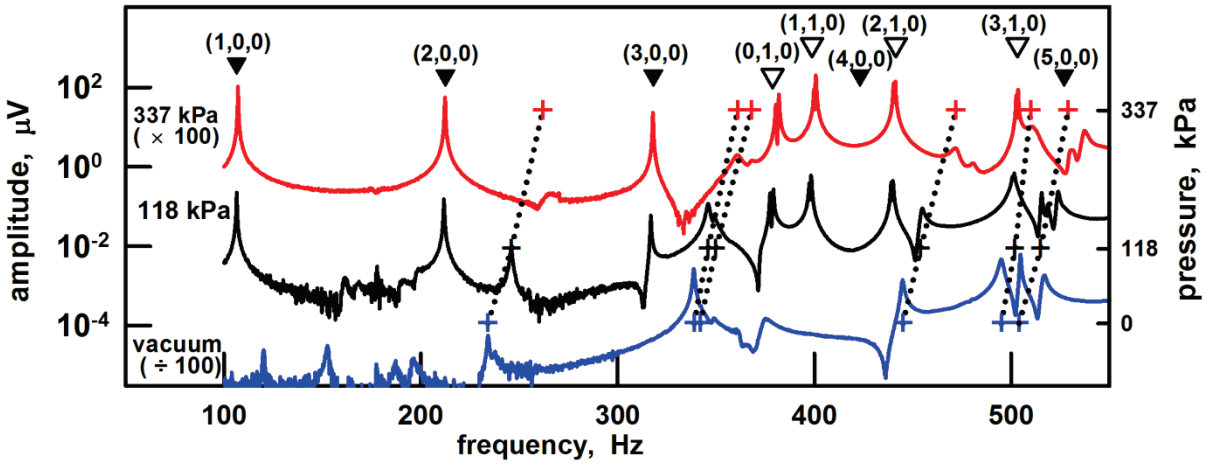

Figure 7. Left Scale: Logarithm of detected acoustic amplitude as a function of frequency for the evacuated tank and for the tank filled with argon. The predicted frequencies f_{calc} of the non-degenerate acoustic modes are indicated by solid triangles; the open triangles indicate f_{calc} of the acoustic doublets. For argon, the values of f_{calc} are independent of pressure on the scale of the figure. For the vacuum data, the measured amplitudes are divided by 100 for plotting; for 340 kPa, the amplitudes were multiplied by 100. Right Scale: Suspected shell resonances are indicated by "+" signs (connected by dotted lines) as a function of pressure.

The vacuum scan in Fig. 7 has high-Q resonances at 234 Hz, 339 Hz, 342 Hz, 445 Hz, 495 Hz, 504 Hz, 560 Hz, and at other frequencies. We identify these resonances as shell resonances and we indicate them in Fig. 7 by plotting blue "+" characters, either just above or just below the vacuum scan. When the pressure in the shell is increased from 0 kPa to 118 kPa and then to 337 kPa, the lower-frequency shell resonances change to higher frequencies and lower Qs. In Fig 7, this frequency change is indicated by dotted lines connecting the "+" characters. We argue that the increase of the shell resonance frequencies with pressure occurred because the pressure-induced tension in the shell made a significant contribution to the "spring constant" for these modes. [16]

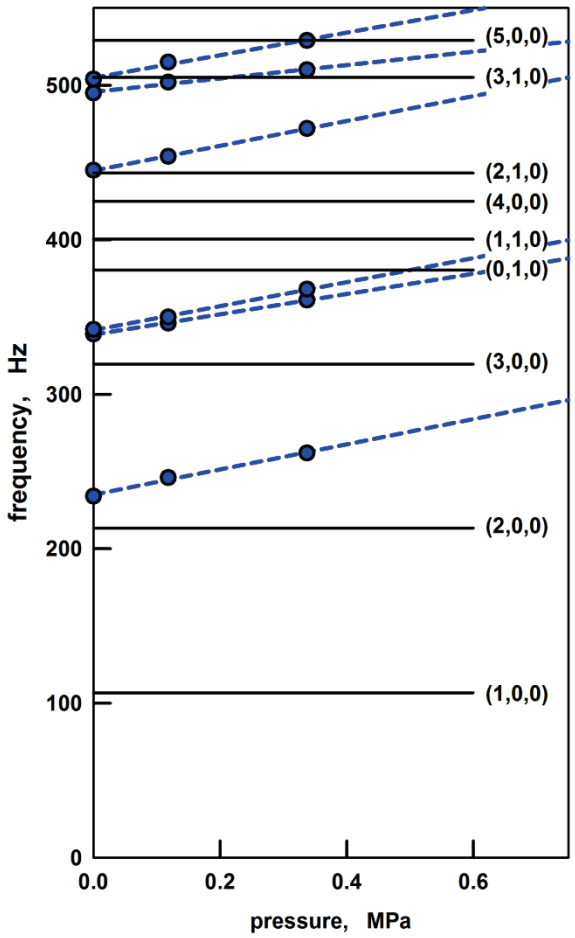

Figure 8. Shell modes (points and dashed lines) and gas modes (solid lines). Note: At $p = 0$, the (2,1,0) gas doublet and the shell mode at 445 Hz nearly cross.

We do not have a model for the coupling between the acoustic transducers and the vibrations of the evacuated tank; therefore, we do not attribute significance to the relative amplitudes of the resonances detected in the vacuum scan. However, we suspect that the resonances of the shell influence the resonances of the gas. Figure 8 shows that, as the pressure increases, the shell modes will cross the gas modes. At low pressures, the 445 Hz shell resonance approaches the (2,1,0) gas resonance. The "avoided `crossing" of these two modes "pushes" the gas resonance to lower frequencies, as shown in greater detail in Fig 9 of [2].

4.3.2. Precise isothermal measurements of acoustic frequencies and half-widths.

We measured the frequencies f_{meas} and half-widths g_{meas} of 7 gas modes at 0.2 MPa, 0.4 MPa, and 0.6 MPa while the tank was on a pallet in a thermostatted laboratory, as shown in figure 1. This set of measurements took two days. As described in Ref. [11], each measurement of f_{meas} and g_{meas} required stepping the frequency of the sound generator up and down through a resonance (or through a doublet) and then fitting resonance functions to the in-phase and quadrature voltages generated by the sound detector. The tabulated data are available from the authors upon request. During these measurements, we recorded the temperatures indicated by two, calibrated, thermistor thermometers. One thermometer was fastened to the top of the tank; the other was fastened to the bottom of the tank. The average of the two thermometers varied slowly between 20.9 °C and 21.9 °C; the temperature difference, $T_{top} - T_{bottom}$ ranged from 0.08 K to -0.04 K.

To compare the measured frequencies f_{meas} with the values of the wavenumbers k_{calc} predicted by the FE models, we formed the ratio $\Re$:

$$\Re = k_{meas}/k_{calc} = 2\pi\left(f_{meas} - \Delta f_{calc}\right)/\left[u(p,T)k_{calc}\right], \quad (10)$$

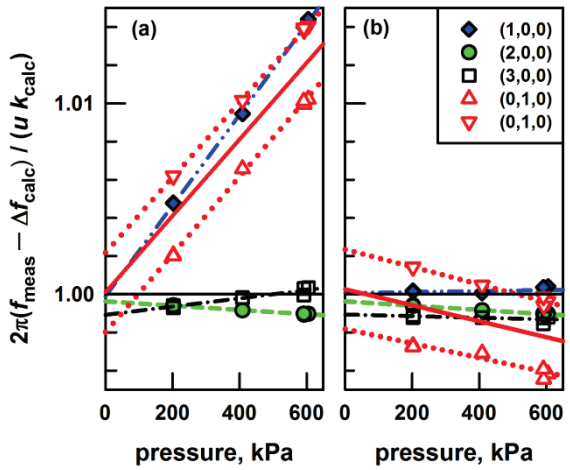

Figure 9. Corrected, measured frequencies ($f_{meas} - \Delta f_{calc}$) divided by calculated frequencies $f_{calc} = [u(p,T)k_{calc}]/(2\pi)$. Left: $\Delta f_{calc} = -g_{calc}$, which is the thermo-acoustic boundary layer correction. Right: $\Delta f_{calc} = -g_{calc} + \Delta f_{CM,1} + \Delta f_{CM,2}$. The CM corrections account for most of the pressure-dependence of the plotted modes. For the (0,1,0) doublet, the solid red line is the average of the dashed lines through each component of the doublet.

which has the value $\Re = 1$ when measurements and calculations agree perfectly. In equation (10), we used values for the speed of sound of argon $u(p,T)$ from Ref. [3]. The frequency-correction term Δf_{calc} in equation (10) always includes the thermo-acoustic boundary correction $\Delta f_{calc} = -g_{calc}$, where $g_{calc} \equiv g_T + g_v$ is the half-width. In the cylinder model (discussed in Section 4.1), this correction is small; its maximum value $g_{calc}/f_{meas} = 0.0006$ occurs for the (1,0,0) mode at 200 kPa and the values decrease as $(pf)^{-1/2}$. Because the correction is small, we estimated it using the cylinder model calculation of g_{calc}.

Figure 9 is a plot of the ratio $\Re(p,T)$ defined by Eq (10) for the 4 lowest-frequency modes that illustrates the effect of the CM corrections. For all the data, we first applied the correction $\Delta f_{calc} = -g_{calc}$, which is always small: $g_{calc}/f_{meas} \le 0.0006$. The data plotted in the left panel omit the CM corrections while the data plotted in the right panel include the CM terms: $\Delta f_{CM,1} + \Delta f_{CM,2}$, where the term CM,1 applies to the modes (1,0,0) and (3,0,0) and the term CM,2 applies to the (0,1,0) doublet. The right panel shows that the CM terms account for nearly all the pressure-dependence visible in the left panel.

Figure 9 also displays the utility of averaging the two components of the (0,1,0) doublet. As $p \to 0$, the average of the two components (solid red line) extrapolates to $\Re = 1.00026$, which is much closer to the theoretical value $\Re = 1$ than the extrapolation of either component.

Figure 10 compares the measured half-widths with the half-widths calculated using the cylinder model for the four lowest-frequency acoustic modes. For all the modes we studied, $g_{meas} \le 7\times10^{-4} f_{meas}$. For the (3,0,0) mode at 200 kPa, $g_{meas} < g_{calc}$. We have no explanation for this anomalous result.

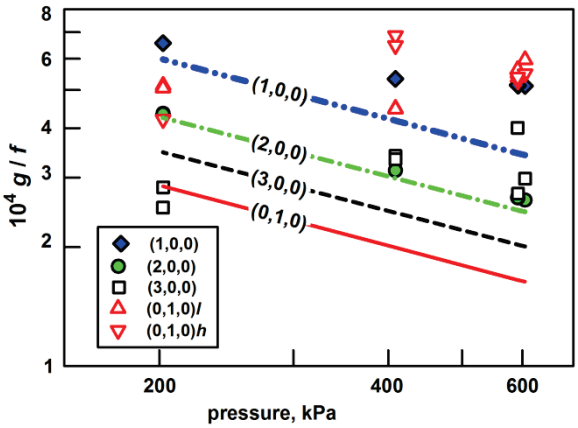

Figure 10. Measured half-widths (points) compared with calculated half-widths (lines). In most cases the measured half-widths exceed the calculated half-widths by a few parts in 10^{-4} of the frequency.

4.3.3. Summary of isothermal results

For 7 low-frequency modes, Fig 11 and table 2 compare the ratio of calculated frequencies (or, equivalently, wavenumbers) to the measured, corrected frequencies at 600 kPa and when extrapolated to zero pressure. The plotted values were determined by averaging the frequencies of the measured doublets and then fitting the averaged frequencies of doublets (and of the singlets) with straight lines, such as those shown in Fig 9. For the 4 lowest-frequency acoustic modes, the average of the zero-pressure values of $\langle k_{meas}/k_{calc}\rangle - 1 = (-0.00028 \pm 0.00059)$, where the uncertainty is one standard deviation. On the scale of Fig 11, the FE results for the spheroidal end-cap model and photo-based model are indistinguishable. The standard deviation of the fractional differences of the measured acoustic frequencies from the calculated frequencies using either FE model is 3.7 times larger than the standard deviation of the fractional differences of the measured microwave frequencies from the models in [1].

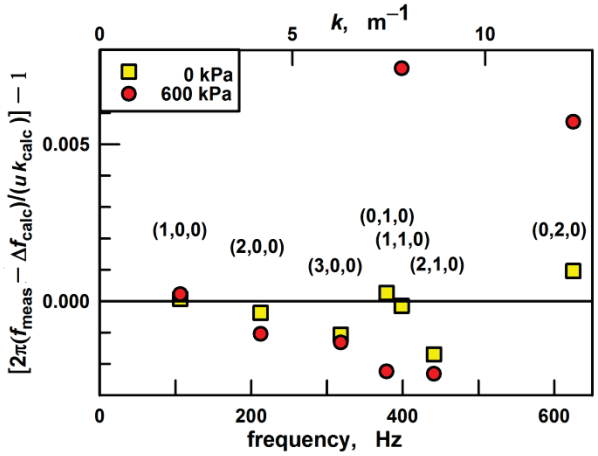

Figure 11. Comparison of measured and calculated (baseline) wavenumbers for 7 modes (after averaging doublets) at 600 kPa and extrapolated to 0 kPa.

At 600 kPa, the acoustic results for the (1,1,0) and (0,2,0) modes differ by more than 0.5 % from the models; therefore these modes of the tank are not suitable for gas metrology. It is plausible that the anomalous behavior of these modes results from the shell modes that occur at 339 Hz and 342 Hz under vacuum and extrapolate to higher frequencies as the pressure is raised. (See figure 8.)

The weighted average of the 4 lowest-frequency acoustic modes in figure 11 is $\langle k_{meas}/k_{calc}\rangle - 1 = (-0.00072 \pm 0.00076)$ at 600 kPa. This implies that these modes, or a subset of them, could be used to determine the speed of sound u in a gas inside the tank with an uncertainty on the order of 0.08 % by calibrating the tank with microwaves alone. From equation (1), the gas's density (and mass) vary as u^{-2}, and their uncertainties will be at least twice the uncertainty of the speed of sound. Therefore, the inconsistency among the 4 lowest-frequency acoustic modes contributes to the uncertainty of M the amount $u_r(M) = 0.0015$ listed in Table 3. Remarkably, the lowest-three acoustic modes have no unexplained pressure-dependence: $\langle k_{meas}/k_{calc}\rangle_{600\ kPa}/\langle k_{meas}/k_{calc}\rangle_{0\ kPa} - 1 = (0.00026 \pm 0.00041)$. These modes are least subject to perturbations from shell resonances.

5. Weighing the Gas in the Tank

In this section, we simulate using the tank as the "bucket" of a "bucket and stopwatch" gas flow standard. Using only microwave calibration data and then {microwave + acoustic} calibration data, we determine the mass of argon in the tank. We consider the effects of temperature gradients and the uncertainy of the collected mass.

5.1. Weighing the collected gas –no temperature gradient

Following [17,18], we assume that the tank was evacuated before the calibration began. To begin a calibration, the operator establishes a steady gas flow through the meter under test into a pipe that bypasses the collection tank. After a steady flow is established, a timer ("stopwatch") is started and, simultaneously, valves are actuated to redirect the flow from the bypass into the collection tank. These operations define the start of the calibration interval Δt. At the end of the interval Δt, the timer is stopped and the valves are actuated to direct the flow back into the bypass pipe. After a much longer interval that allows the collected gas to come into a steady state, the mass M of the collected gas is determined from pressure and temperature measurements and a prior calibration of the tank's volume. Finally, the mass flow rate $Q = M/\Delta t$ is computed.

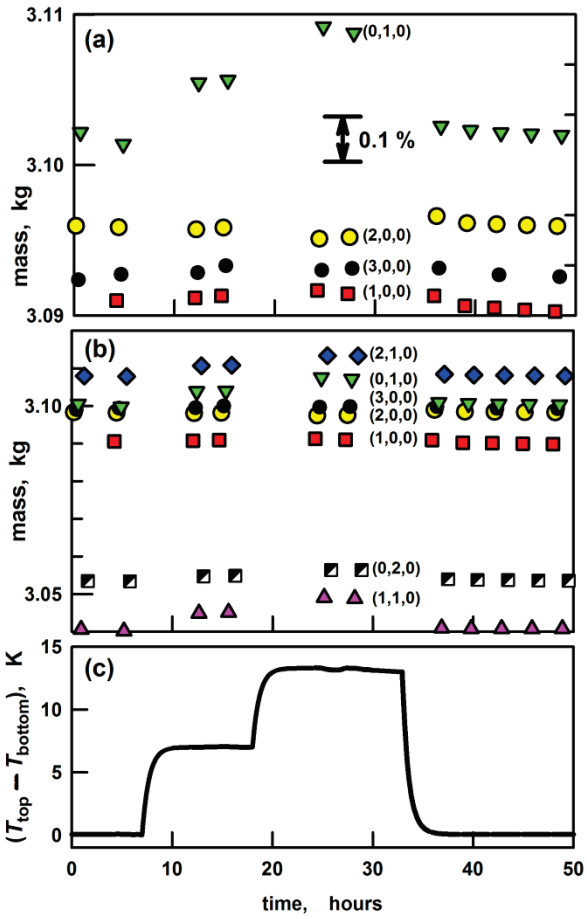

Figure 12. (c): Temperature differences $\Delta T \equiv T_{top} - T_{bottom}$ imposed on the tank during a 2-day interval. (a): Mass measurements during 2 days using $p = 0$ acoustic wavenumbers determined in figure 11. (b) Simulated mass measurement using wavenumbers for 7 acoustic modes computed from microwave data. Note: When $\Delta T = 13$ K, the fractional changes in the computed mass in (a) and (b) were $|\Delta M/M| \le 0.00013$ for the longitudinal modes (1,0,0), (2,0,0), (3,0,0) and $|\Delta M/M| \le 0.0014$ for the averaged doublets.

Our simulation assumes that (1) the mass of the tank is known, (2) the microwave measurements and model have been completed, (3) after the collection is completed, the acoustic resonance frequencies and the pressure are measured, (4) the thermophysical properties of argon are accurately known, and (5), in this case, the collected gas was at a pressure of 0.6 MPa. In the simulation, we did not attempt to correct for the unmodeled pressure-dependence of the resonance frequencies that we observed under nearly isothermal conditions. However, guided by our observation that shell modes and the gas modes interact, we used only the lowest-frequency acoustic modes.

The center (b) panel of figure 12 displays the mass M of argon in the tank deduced from the pressure and from the frequencies and wavenumbers of the various acoustic modes, as outlined in figure 2. The calculations used the thermophysical property data for argon from [3]. In the absence of a temperature gradient, the mean and standard deviation of the density for the 4 lowest-frequency acoustic modes was: $\langle\langle\rho\rangle\rangle_{4modes} = 10.478\times(1 \pm 0.0014)$ kg/m^3. Using V_{tank} from the microwave measurements, we found the mass of argon in the tank $M = \langle\langle\rho\rangle\rangle_{4modes} V_{tank} = 3.0979\times(1 \pm 0.0016)$ kg, where the uncertainty includes all the terms in table 3 below.

In figure 12, the upper-most panel 12(a) displays the same data as 12(b); however, the analysis used the wavenumbers that we deduced from the isothermal acoustic measurements in Section 4.3 instead of the wavenumbers calculated from the microwave measurements. If this kind of calibration (using an isothermal reference gas, such as argon) were available and if only the lowest three acoustic modes were used, the fractional standard deviation of M for the test gas would be reduced from 0.0016 to 0.0007, even if the measurements were made with a temperature gradient.

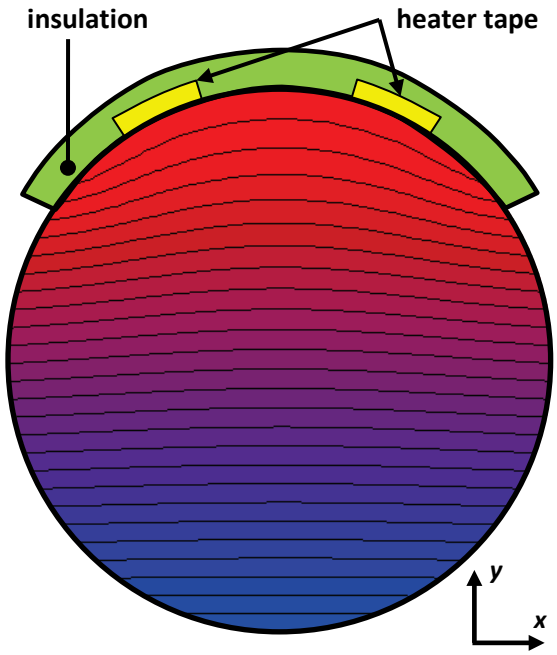

Figure 13. Non-uniform, vertical temperature gradient imposed by heater tape and insulation.

5.2. Effects of a temperature gradient

5.2.1. Predictions from theory

When the temperature T is a function of position within the volume of gas in the tank, the speed of sound u in the gas will be a function of position as well. Sound waves will travel faster in warmer regions of the tank and slower in cooler regions. This variation in the speed of sound affects the distance that sound waves travel as they propagate through the volume, and thereby changes the frequencies at which resonance occurs. The amount by which the resonance frequency is changed depends on the symmetry of the mode and on the symmetry of the temperature field. To develop insight into how the resonance frequencies change when a temperature gradient is imposed, we used first-order perturbation theory to calculate the resonance frequencies of a rigid, perfectly cylindrical cavity with a model temperature gradient (see Fig. 13) that resembles the gradient generated in the laboratory (Section 5.2.2, below). (The calculation ignores the thermal expansion and contraction of different parts of the shell that change the shape of a real cavity.) Details of the calculations and the results are described elsewhere. [2,19]

We calculated the fractional frequency changes for 7 modes with the temperature differences ΔT = 7 K and 13 K that were used in our measurements. For our model temperature profile, the calculations predict that the frequencies of non-degenerate modes and the averaged frequency of doublets are unchanged by the temperature gradient to first order in $\Delta T/T$.

In the next section, we discuss measurements of frequency changes generated by temperature gradients. For the non-degenerate (1,0,0), (2,0,0) and (3,0,0) modes, the measured frequency changes are small and irregular: $|\Delta f_{\mathrm{meas}}/f_{\mathrm{meas}}| \le 1.3\times10^{-4}$. For these three modes at ΔT = 13 K, the average and standard deviation of the frequency changes were $\Delta f_{\mathrm{meas}}/f_{\mathrm{meas}} = (0.2 \pm 1.3)\times10^{-4}$ K. This null result is consistent with the perturbation calculation result that the first-order frequency change is zero.

For the degenerate modes, the values of $\Delta f_{\mathrm{meas}}/f_{\mathrm{meas}}$ are as large as 14×10^{-4} and they are consistent with the linear dependence $\Delta f_{\mathrm{meas}}/f_{\mathrm{meas}} \propto \Delta T$. We present evidence that the measured linear dependence of

$\Delta f_{meas}/f_{meas}$ on ΔT for the doublets resulted from a change in the shape of the tank that was produced by the asymmetric heating.

5.2.2. Measurements in a temperature gradient

We document the need to account for temperature gradients in a large collector tank by quoting from Ref. [18], which describes the 26 m^3 tank at NIST:

> "The predominant source of uncertainty in the average gas temperature results from spatial temperature variations of the gas inside the collection tank. These temperature inhomogeneities derive from two sources: (1) inhomogeneities imposed on the gas from temperature gradients in the room surrounding the collection tank; and (2) residual temperature inhomogeneities remaining in the collected gas resulting from the evacuation and filling processes of a flow measurement cycle. Given sufficient time, the temperature gradients in the gas caused by the calibration cycle decay; however, the gradients imposed by the room persist."

Within a few minutes after the collection stops, bouyancy-driven convection stratifies the gas in the collection tank so that the warmer gas is near the top of the tank and cooler gas is near the bottom of the tank. Subsequent temperature changes can take hours.

As shown schematically in figure 13, the top quarter of the tank was covered with an insulating blanket. Beneath the blanket, we had taped a heater to the top of the tank and a thermistor that was used to estimate the temperature T_{top}. A second thermistor taped to the bottom of the tank estimated T_{bottom}. Figure 12(c) displays the time-dependence of the temperature difference $\Delta T = (T_{top} - T_{bottom})$. During hours 7 to 17 we applied 120 W to the heater. This generated an approximately-vertical, non-uniform, temperature gradient in the tank such that T_{top} = 30.8 °C, T_{bottom} = 23.8 °C, and the average temperature acoustic temperature $\langle T_{acoust} \rangle$ = 26.5 °C. During hours 17 and 30, we applied 240 W to the heater and generated a nearly-steady-state with T_{top} = 39.7 °C, T_{bottom} = 26.4 °C, and $\langle T_{acoust} \rangle$ = 31.8 °C. The maximum measured temperature difference was, fractionally, $\Delta T/T \approx 0.043$; however, there could have been larger temperature differences between locations on the tank that were not detected by the two thermometers. During the 50 h spanned by figure 12, the temperature of the laboratory varied by approximately ±0.5 K.

Table 2 of [2] compares the measured frequency changes caused by the heater with the changes predicted by the cylinder model using first-order perturbation theory. Independent of any model, it is remarkable that a temperature gradient on the order of $\Delta T/T \approx 0.043$ which changes the speed of sound in argon by $\Delta u/u \approx 0.043/2$ generated a resonance frequency change $|\Delta f/f| \leq 0.00126$ in the worst case. For the non-degenerate longitudinal modes, (1,0,0), (2,0,0), and (3,0,0), the measured frequency changes were compartively small and noisy:$10^4|\Delta f/f| \leq 2.4$. Thus, these changes are on the order of $(\Delta T/T)^2$. For the averaged doublets, the frequency changes were as large as $10^4|\Delta f/f| \leq 12.6$ and consistent with a linear dependence on the temperature difference. As discussed above and in Section 3.3 of [2], a 1st order model predicts $\Delta f/f = 0$ for the non-degenrate modes and for the averaged doublets. The 2nd order model also predicts $\Delta f/f = 0$ for the non-degenerate modes and $\Delta f/f \propto (\Delta T)^2$ with very small coefficients of proportionality for the doublets. The inconsistency between the measurements and the model led us to examine the effect of the temperature gradient on the shape of the cavity, as estimated from the microwave frequencies and from a FE model of a long cylinder.

For 10 microwave doublets, figure 14 displays the changes of the average frequencies and the frequency splittings from reference values when the temperature gradient was imposed. The reference values were measured during the interval from 3 h to 4 h, while the temperature of the tank was T_{ref} = 21.2 °C and the heater power was zero. Before plotting, the averaged frequencies f_{av} were reduced by $\alpha_T[(T_{top}+T_{bottom})/2-T_{ref}]$ to account for the linear coefficient of thermal expansion of the tank measured in [1]. The data for the averaged doublets (middle panel of figure 14) have the mean value and standard deviation $\langle(f_{av}-f_{av,ref})/f_{av}\rangle = 2.6\times10^{-5}$ and $\sigma[(f_{av}-f_{av,ref})/f_{av}] = 8.1\times10^{-5}$, when $\Delta T = (T_{top}-T_{bottom}) = 13$ K. They are consistent with the linear relation $(f_{av}-f_{av,ref})/f_{av} \propto \Delta T$ with coefficients of proportionality ranging from -3.3×10^{-6} K^{-1} to 1.5×10^{-5} K^{-1}. The data for the splitting of the doublets (top panel of figure 13) are also consistent with the linear relation $(f_{split}-f_{split,ref})/f_{av} \propto \Delta T$ with much larger coefficients of proportionality ranging from -7.4×10^{-5} K^{-1} to 1.5×10^{-5} K^{-1}. We now argue that these data cannot be explained by redistribution of the argon caused by temperature gradients.

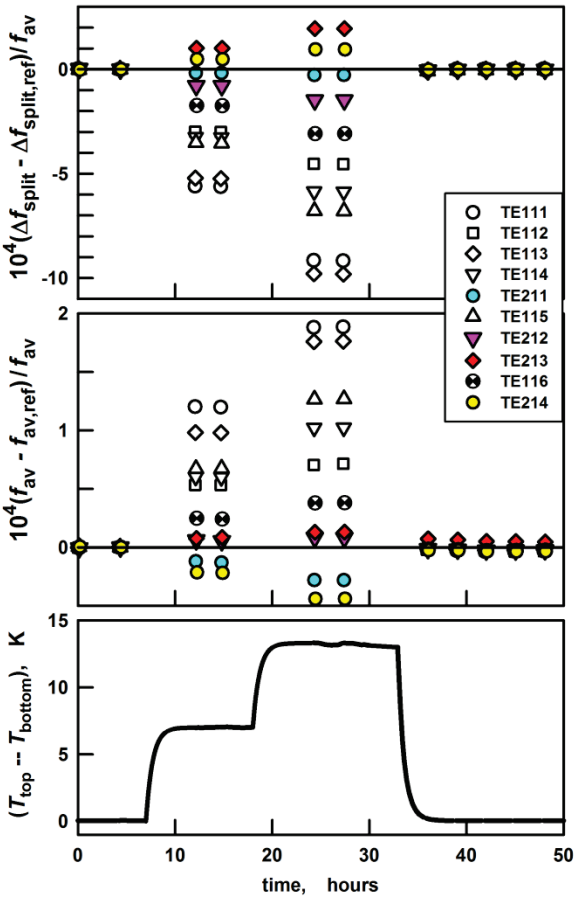

Figure 14. Bottom: Vertical temperature differences imposed on the tank during a 2-day-long interval. Center: fractional frequency changes $(\Delta f/f)_{microwave}$ of averaged microwave doublets caused by temperature gradients. Top: changes in the splitting of the doublets caused by gradients. For each mode, the value of the frequency and splitting near the 4 hour mark is used as the reference.

During the measurements shown in figure 14, the refractive index of the argon was $n \approx 1 + 3A_\varepsilon\rho \approx 1.00163$, where $A_\varepsilon = 4.142$ cm^{3}mol^{-1} is the dielectric polarizability of argon. [20] The largest temperature difference, $\Delta T/T \approx 0.043$, redistributed the argon within the tank and changed the refractive index *locally* by, at most, $\Delta n \approx (n-1)\Delta\rho/\rho \approx (n-1)(-\Delta T/T) \approx -7\times10^{-5}$. The microwave frequencies, similar to the acoustic frequencies discussed in Section 3.3, depend upon volume averages of the density; therefore, we expected the frequency changes $(\Delta f/f)_{micro}$ to be much less than 7×10^{-5}. Furthermore, the temperature-gradient-driven changes of $(\Delta f/f)_{micro}$ for the averaged doublets are expected to vary as $(\Delta T/T)^2$, not as $(\Delta T/T)$.

We used a FlexPDE script for thermoelasticity problems to estimate the effects of a uniform, vertical temperature gradient on a long, horizontal, cylindrical shell with unconstrained boundaries and with the properties: inner radius 0.25 m, thickness 3.9 mm, Young's modulus 197 GPa, Poisson ratio 0.297, and linear coefficient of thermal expansion 12×10^{-6} K^{-1}. As a measure of the effect of a temperature difference $\Delta T = T_{top}-T_{bottom}$, we used the ratio l_v/l_h, where l_v and l_h are the lengths of the semi-major vertical and horizontal axes of the cylinder's cross-section. This FE model predicts $l_v/l_h = 1+6.1\times10^{-6}(\Delta T/\text{K})$. For ΔT

= 13 K, $l_v/l_h = 1.000079$, which is on the order of the values of $(\Delta f/f)_{microwave}$ in figure 14. This order-of-magnitude agreement supports the idea that the imposed temperature gradient changes the shape of the tank and the shape change leads to the linear relation $(\Delta f/f)_{microwave} \propto (\Delta T/T)$. In a future publication, we will test this idea quantitatively.

5.3. Uncertainties

Table 3 summarizes the contributions to the uncertainty of the present determination of the mass of argon in the tank in the presence of a temperature gradient.

We do not have a model for shape changes induced by temperature gradients; therefore, such changes contribute to the uncertainty of the mass measurement. We estimate this contribution by using equation (1) and neglecting the real-gas corrections: $M \propto V_{tank}/u^2 \propto (f_{micro})^3/(f_{acoust})^2$. On the average, the unmodeled shape change affects the acoustic and microwave frequencies (or, equivalently, wavenumbers) by the same fraction; therefore we use the standard deviation $\sigma[(\Delta f/f)_{micro}] = 8.1\times10^{-5}$ when $(T_{top} - T_{bottom}) = 13$ K as a measure of this uncertainty contribution.

In Ref. [1], we showed that, as the pressure inside the tank was increased, the expansion of V_{tank} was not isotropic; however, we did not develop a quantitative model for the expansion. Instead, we argued that the pressure expansion was greater than that of a thin-walled spherical shell and less than that of a long, thin-walled, cylindrical shell to arrive at the lower and upper bounds: $3.5\times10^{-4}\ \text{MPa}^{-1} < (\partial V/\partial p)_T/V < 6.2\times10^{-4}\ \text{MPa}^{-1}$. For a pressure change of 0.6 MPa, the difference between these two bounds is 2×10^{-4}, which we take as the fractional uncertainty of V_{tank} upon increasing the internal pressure.

We obtained the thermodynamic data for argon from the Helmholtz energy surface developed by Tegeler *et al.* [3] Their surface reproduces the accurate speed-of-sound data of Estrada-Alexanders and Trusler [21] with a fractional uncertainty $u_r(u) = 7\times10^{-5}$ or less, over a wide range of conditions including those encountered here. The mass of argon in the tank is calculated from u^2; therefore, we estimate the thermodynamic contribution to $u_r(M)$ as $2\times u_r(u) = 1.4\times10^{-4}$. This uncertainty could be reduced if the argon data were re-analyzed using the density and acoustic virial coefficients deduced from *ab initio* theory [11].

During the present measurements, we used two pressure gauges. Based on the manufacturer's specifications and our experience with these gauges, we estimated $u_r(p) = 0.0001$ near 0.6 MPa.

Table 3. Estimated fractional uncertainty of M with coverage factor $k = 1$.

phenomenon	estimate	value
Volume of empty tank	Ref. [1]	0.0006
Volume increase between 0 MPa and 0.6 MPa	Sect. 5.2	0.0002
Inconsistent acoustic modes at 0.6 MPa	Sect. 4.3.3	0.0015
Speed of sound in argon at 0.6 MPa	Ref. [3]	0.00014
Pressure		0.0001
Unmodeled shape change at $(T_{top}-T_{bottom}) = 13$ K	Sect. 5.2	0.00008
Root Sum of Squares		0.0016

6. Discussion: Prospects for a Large Flow Standard

We simulated a "bucket and stopwatch" flow calibration using a collection tank with a volume that was determined (while evacuated) from measurements of the frequencies of its microwave resonances. We determined the mass of argon in the tank by measuring the pressure and the frequencies of the acoustic resonances in the argon. The relative uncertainty of the collected mass was $u_r(M) = 0.0016$, where the uncertainty was dominated by inconsistent results from the three lowest-frequency acoustic modes. The value of the collected mass, determined acoustically, was only weakly sensitive to temperature gradients imposed on the collection tank. We now discuss strategies for reducing the uncertainty, problems that might arise upon increasing V_{tank} by a factor of 10 to 100, and problems that might arise when using the collection tank as part of a dynamic flow standard: that is, a standard that measures the collected mass while gas is flowing into the tank.

As mentioned in Section 4.1 and suggested by figure 8, the inconsistencies among the acoustic wavenumbers might have resulted from the effects of un-modeled shell resonances that were detected during the vacuum measurements in figure 7. We determined experimental values of the acoustic wavenumbers by assuming, for each mode, the values of $(f_{meas} + g_{calc})_{lmn}$ are linear functions of the pressure and we extrapolated these values to zero pressure. This procedure has worked remarkably well for thick shells [11] when the frequencies of the shell resonances are nearly constant over the relevant pressure range. However, the resonance frequencies of thin-walled shells are stronger functions of pressure; therefore, the assumption of linearity is questionable. More accurate wavenumbers might be obtained by using a better model for extrapolating to zero pressure and/or by using a thicker shell. In this context, a spherical shell is advantageous because it is approximately twice as stiff as a cylindrical shell with the same thickness-to-radius ratio.

If the volume of the collection tank were increased by a factor of 10 to 100, the cost of a well-characterized test gas, such as pure argon, might be significant. If less-well-characterized test gases were used, (for example, a natural gas with, possibly, varying composition), it might be necessary to measure the speed of sound of the test gas using a small, auxiliary, thermostatted acoustic resonator under conditions encountered in the flow standard. If the auxiliary resonator were a suitably-designed Helmholtz resonator, it could operate in the same frequency range as the collection tank.

To achieve similar signal-to-noise ratios using the lower-frequency modes of a 10× to 100× larger volume tank, the microwave power and acoustic power would have to be increased by factors of approximately 10× to 100×. (Here, we neglect the size-dependence of the Qs.) Fortunately, the accuracy of the present mass determination was not limited by the signal-to-noise ratio of either the microwave or acoustic measurements; therefore sufficient accuracy may be obtained from larger tanks without scaling the power.

While we conducted our acoustic measurements, all of the tank's ports were closed. It might be desirable to conduct "dynamic" calibrations, that is, calibrations conducted while gas flowed through a duct, either into or out of the collection tank. In the absence of flow, such ducts would have only small effects on the acoustic resonance frequencies of modes that had pressure nodes where the ducts connected to the tank. However, the effects of flow on the resonance frequencies should be a subject for future research.

A constraint applicable to dynamic calibrations is the time required to accurately measure an acoustic resonance frequency. When a sound generator operating at a frequency near a cavity resonance f_N is turned

on at the time $t = 0$, the acoustic pressure approaches a steady-state value as $\exp(-2\pi g_N t)$, where g_N is the half-width of the resonance. If we apply the conservative criterion, $\exp(-2\pi g_N t) < 10^{-4}$, under the conditions of figure 12 ($g_{(1,0,0)} \approx g_{(2,0,0)} \approx 0.06$ Hz) a wait of $t = 24$ s is required before each amplitude measurement. In this work, we used a very conservative protocol that determined f_N and g_N by fitting 22 amplitudes. The amplitudes were measured at 11 frequencies starting at $f_N - g_N$ and ending at $f_N + g_N$ with steps of $g_N/5$. Then, the frequency sweep was reversed, starting at $f_N + g_N$ and ending at $f_N - g_N$ with steps of $-g_N/5$. This protocol requires 528 s for a mode such as (1,0,0) with $g_{1,0,0} = 0.06$ Hz. Other protocols can be devised; however, the characteristic time $(2\pi g_N)^{-1}$ is inherent in any resonance method.

Acknowledgements

We thank John D Wright for his continuing support and his help in conducting the gas expansion measurement of the tank's volume.

References:

[1] M. R. Moldover, J. W. Schmidt, K. A. Gillis, J. B. Mehl and J. D. Wright, "Microwave determination of the volume of a pressure vessel," *Meas. Sci. Tech*. **26**, 015304 (2015).

[2] Gillis K A, Mehl J B, Schmidt J W, and Moldover M R 2015 "'Weighing' a gas with microwave and acoustic resonances" (accepted for publication in *Metrologia*).

[3] Ch. Tegeler, R. Span, and W. Wagner, "A new equation of state for argon covering the fluid region for temperatures from the melting line to 700 K at pressures up to 1000 MPa," *J. Phys. Chem. Ref. Data* **28**, 779-850 (1999), as implemented in the computer package: E. W. Lemmon, M. O. McLinden, and M. L. Huber, "REFPROP: Reference Fluid Thermodynamic and Transport Properties," NIST Standard Reference Database 23, Version 9.1, Natl. Inst. Stand. and Tech., Boulder, CO, (2010) www.nist.gov/srd/nist23.cfm

[4] K. A. Gillis, "Thermodynamic properties of two gaseous halogenated ethers from speed-of-sound measurements: difluoromethoxy-difluoromethane and 2-difluoromethoxy-1,1,1-drifluoroethane," *Intl J. Thermophysics* **15**, 821-47 (1994).

[5] Span, R., Lemmon, E.W., Jacobsen, R.T, Wagner, W., and Yokozeki, A. "A Reference Equation of State for the Thermodynamic Properties of Nitrogen for Temperatures from 63.151 to 1000 K and Pressures to 2200 MPa," *J. Phys. Chem. Ref. Data*, **29**, 1361-1433, (2000), as implemented in the computer package: E. W. Lemmon, M. O. McLinden, and M. L. Huber, "REFPROP: Reference Fluid Thermodynamic and Transport Properties," NIST Standard Reference Database 23, Version 9.1, Natl. Inst. Stand. and Tech., Boulder, CO, (2010) www.nist.gov/srd/nist23.cfm

[6] Wright J D, 2004 *34 L and 677 L PVTt volume determinations and description of system changes* (Gaithersburg, MD, USA: National Institute of Standards and Technology, internal report dated 3 March 2004)

[7] Jackson J D 1975 *Classical Electrodynamics* (New York: John Wiley & Sons) pp 339-60

[8] Collin R F 1966 *Foundations of Microwave Engineering* (New York: John Wiley & Sons) pp 504-8

[9] Underwood R J and Edwards G J 2014 Microwave-dimensional measurements of cylindrical resonators for primary acoustic thermometry *Int. J. Thermophysics* **35** 971-84

[10] H. Feshbach, "On the perturbation of boundary conditions," *Phys. Rev.* **65**, 307-18 (1944).

[11] Moldover M R, Gavioso R M, Mehl J B, Pitre L, de Podesta M, and Zhang J T 2014 Acoustic gas thermometry *Metrologia* **51** R1-R19

[12] COMSOL Multiphysics version 4.2a, 1998-2011 COMSOL AB (www.comsol.com)

[13] FlexPDE version 6.36 released 29 Jul 2014, PDE Solutions, Inc., Spokane Valley, WA, USA (www.pdesolutions.com)

[14] ASME Boiler and Pressure Vessel Code, Section II - Materials, Part D - Properties (Metric) 2010 (New York: American Society of Mechanical Engineers)

[15] Hearn E J 1997 *Mechanics of Materials* (Oxford: Butter-worth-Heinemann) pp 201-2

[16] Y. C. Fung, E. E. Sechlere, and A. Kaplan, "On the vibration of thin cylindrical shells under internal pressure," *J of the Aeronautical Sciences* **24**, 650-60 (1957).

[17] J. D. Wright, A. N. Johnson, and M. R. Moldover, "Design and uncertainty analysis for a PVTt gas flow standard," *J. Res. Nat. Inst. Standards Technology* **108**, 21-47 (2003).

[18] A. N. Johnson, J. D. Wright, M. R. Moldover, and P. I. Espina, "Temperature characterization in the collection tank of the NIST 26 m^3 *PVTt* gas flow standard," *Metrologia* **40**, 211-16 (2003).

[19] K. A. Gillis, J. B. Mehl, and M.R. Moldover, "Effect of a temperature gradient on the modes of a cylindrical chamber: perturbation theory," in preparation.

[20] J. W. Schmidt, and M. R. Moldover, "Dielectric permittivity of eight gases measured with cross capacitors," *Int. J. Thermophysics* **24**, 375-403 (2003).

[21] A. F. Estrada-Alexanders and J. P. M. Trusler, "Thermodynamic properties of gaseous argon at temperatures between 110 and 450 K and densities up to 6.8 mol•dm^{-3} determined from the speed of sound," *Int. J. Thermophys.* **17**, 1325-13 (1996).